PNAS
www.pnas.org

Supplementary Information For:

TITLE: Th17 lymphocytes drive vascular and neuronal deficits in a mouse model of postinfectious autoimmune encephalitis

AUTHORS: Maryann P. Platt[1,2], Kevin A. Bolding[3], Charlotte R. Wayne[2,4], Sarah Chaudhry[2], Tyler Cutforth[2], Kevin M. Franks[3,7] and Dritan Agalliu[2,5,6,7]

AUTHOR AFFILIATIONS:

1. Graduate Program in Neurobiology and Behavior, Columbia University Irving Medical Center (CUIMC), New York, NY, 10032 USA
2. Department of Neurology, CUIMC
3. Department of Neurobiology, Duke University Medical Center, Durham, NC, 27708 USA
4. Integrated Program in Cellular, Molecular and Biomedical Studies, CUIMC
5. Department of Pathology and Cell Biology, CUIMC
6. Lead contact: Dritan Agalliu, Ph.D.
   E-mail: da191@cumc.columbia.edu
   Address: Department of Neurology, Columbia University Irving Medical Center, 650 West 168th Street, Black Building, Room 310E, New York, NY 10032
   Telephone: 212-305-0323
   Facsimile: 212-305-0246

7. **CORRESPONDING AUTHORS:** da191@cumc.columbia.edu (D.A) and franks@neuro.duke.edu (K.F.)

This PDF file includes:

Supplementary Information Text
Figures S1 to S7
References for SI Reference Citations

www.pnas.org/cgi/doi/10.1073/pnas.1911097117

SUPPLEMENTARY INFORMATION TEXT

Supplementary Methods

Mice. All procedures were approved by the Institutional Care and Use Committees of Columbia University Irving Medical Center (CUIMC; #AAAX3452) and Duke University (#A220-15-08). Postnatal day 28 (P28) SJL/J female mice were purchased from the Jackson Laboratory (000686, the Jackson Laboratory, Bar Harbor, ME). Male and female *RORγt*$^{+/GFP}$ and *RORγt*$^{GFP/GFP}$ mice (*B6.129P2(Cg)-Rorc*^{tm2Litt}*/J*) (1, 2), purchased from the Jackson Laboratory, were backcrossed to C57BL/6J mice for 5 generations at CUIMC prior to breeding for experiments.

GAS intranasal infections: SJL/J, *RORγt*$^{+/GFP}$ and *RORγt*$^{GFP/GFP}$ female mice received five weekly intranasal (i.n.) GAS infections as described (3), beginning at postnatal ages 21-28 (P21-P28). Briefly, log phase GAS cultures ($2x10^8$ CFU) were harvested, washed once in sterile phosphate buffered saline (PBS) then resuspended in 100 μl PBS for inoculation by passive inhalation. This modified protocol minimizes death from sepsis and reduces the chance of bacterial aspiration into the lungs during i.n. infection in young mice.

Group A Streptococci (GAS) (*S. pyogenes*) subcutaneous immunizations: SJL/J mice were immunized subcutaneously (s.c.) as described (4-6). Briefly, mice received 100 μl injections of 100 μl heat-killed (HK) GAS pellet homogenized with complete Freund's adjuvant (CFA) containing 200 μg Mycobacterium tuberculosis H37Ra (Difco Labs). Mice received 100 μl injections of emulsion every two weeks for a total of three immunizations. During the first round of immunizations (day 0), mice received an intravenous injection of 400 ng *Bordetella pertussis* toxin (List Biological Laboratories).

Flow cytometry: Mice used for flow cytometry received four live GAS infections and an equal amount of heat-killed GAS (HK-GAS) for the fifth (last) infection, to protect the experimenter during tissue dissections. Mice were anesthetized with isoflurane and perfused with ice-cold sterile PBS. Lymphocytes were isolated as described (7). For cytokine staining, cells were stimulated *in vitro* with eBioscience™ 500 X Cell Stimulation Cocktail (00-4975-03) diluted in T cell media for 4 hours. Cells were then treated with CD16/CD32 Fc block for 1 hour (BD Pharmingen 553141, 1:200) and stained with the following cell surface antibodies for T cell antigens: anti-CD4 BV605 (BD Horizon 562891, 1:100), anti-CD45 BV421 (BD Horizon 563890, 1:100) and eBioscience Fixable Viability Dye eFluor 780 (eBioscience 65-0865-14, 1:2000). For detection of B cells, cells were stained with the following cell surface antibodies: anti-CD45 BUV395 (BD Horizon, 564279, 1:100), anti-CD3 Alexa 700 (BioLegend, 100215, 1:100), anti-CD19 PE-Cy7 (BD Pharmingen, 561739, 1:200), anti-B220 PE-CF594 (BD Horizon, 562313, 1:100). Cells were then fixed and permeabilized using the BD Cytofix/Cytoperm kit (BD Pharmingen 554714). Intracellular cytokines were analyzed by staining with anti-IL-17A PE (BD Pharmingen 559502) anti-IFN-γ APC (BD Pharmingen 554413) antibodies diluted 1:100. For regulatory T cell (Treg) analyses, cells were collected and stained for the same surface antigens without re-stimulation *in vitro*, then fixed, permeabilized (eBiosciences Transcription Factor Fixation/ Permeabilization kit, #512343 and #522356) and stained with an anti-FoxP3 PerCP-Cy5.5 antibody (eBioscience 45-5773-80, 1:100). All flow cytometry analysis was performed on a BD FACS Celesta (Columbia Stem Cell Initiative, Flow Cytometry Core). Gates for cytokine staining were set using fluorescence-minus-one controls and analyzed in FlowJo software (See Figure S2 for gating strategies).

Immunofluorescence: For immunofluorescence analysis, mice were anesthetized with isoflurane and perfused thoroughly with PBS followed by 4% paraformaldehyde (PFA). Brains were extracted and post-fixed for 6 hours in 4% PFA, washed three times with PBS, cryoprotected in 30% sucrose/PBS overnight, and embedded in Tissue Plus O.C.T. compound (ThermoFisher Cat# 4585). Brains were sectioned at 12 μm on a Leica cryostat. Tissue sections were stained with the following primary antibodies: anti-Caveolin1 (1:2000, Abcam), anti-vGluT2 (1:2000, Millipore), anti-GAD67 (1:1000, Abcam), anti-CD4 (1:100, BD Pharmingen), anti-Iba1 (1:500, WAKO), anti-CD68 (1:2000, Abcam), anti-Claudin5 (1:500, Invitrogen), anti-ZO1 (1:500, ThermoFisher), anti-GFP (1:200, Life Technologies), anti-GLUT1 (1:4000, Millipore), anti-Occludin (1:500, Invitrogen), anti-OMP (1:2000, WAKO), anti-Group A Streptococcus (1:2000, Fitzgerald), and BSL-FITC (1:200, Vector Laboratories). Primary antibodies were visualized using fluorescently tagged secondary antibodies (1:1000 for AlexaFluor488 and AlexaFluor594, 1:500 for AlexaFluor647; Life Technologies). Biocytin-TMR fluorescence was amplified with streptavidin conjugated to AlexaFluor594 (1:1000, Life Technologies). Imaging of brain sections was performed with either a Zeiss LSM700 confocal microscope or Zeiss AxioImager fluorescent microscope. Hematoxylin and Eosin staining of the olfactory bulb (OB) sections was performed by the CUIMC Histology Core facility using standard protocols and images were acquired with a Zeiss AxioImager fluorescent microscope.

Microglial quantification: Tiled images of OB sections corresponding to bregmas +4.5, +4.28, and +3.8 were acquired on a Zeiss AxioImager fluorescent microscope. Images were manually counted for $CD68^+$ $Iba1^+$ cells within the glomerular layer of the OB as described (3) with values averaged for three sections. DAPI staining was used to identify the glomeruli. Microglia ($Iba1^+$) were considered activated if their cell bodies were round, contained >50% $CD68^+$ area and had short processes. Highly ramified $Iba1^+$ microglial cell bodies with small $CD68^+$ staining area were not considered activated and therefore they were not included in the analysis. Only microglia within the glomerular layer of the OB were included in this analysis.

Blood-brain barrier (BBB) permeability assessment: Paracellular and transcellular (the rate of endothelial transcytosis) BBB permeability were assessed using intravenous injection of either a small molecular weight tracer, biocytin-tetramethylrhodamine (biocytin-TMR, ThermoFisher Scientific Cat# T12921) or a larger molecular weight tracer albumin-Alexa594 (ThermoFisher Cat# A13101) as described (3, 7-9). Animals were anesthetized with isoflurane 48 hours after the last (fifth) GAS infection and injected with 100 μl (5 mg/ml) biocytin-TMR, albumin-Alexa594, dissolved in D-PBS with Ca^{2+}/Mg^{2+}. IgG leakage was assessed with a single injection of Alexa488-labelled mouse IgG (Bio-Rad Cat# MCA1209A488). The tracers or exogenous mouse IgG were allowed to circulate in the blood for 30 minutes prior to perfusion of animals and tissue fixation. Brain or liver sections were imaged in a Zeiss LSM700 confocal microscope to detect extravasation of either biocytin-TMR or albumin Alexa-594 in the tissue or endothelial uptake of albumin-AlexaFluor594. Analysis of biocytin-TMR distribution and fluorescence intensity in various brain and liver regions was performed as described (3, 7-9). Briefly, 8-12 fields of view (FOV) were acquired from at least 3 OB sections for the analysis of biocytin-TMR and albumin-AlexaFluor594 extravasation. Biocytin-TMR fluorescence intensity was measured for 10 linear selections along a 30 μm line drawn perpendicular to a blood vessel, excluding the vessel. Vascular albumin uptake was measured in the FOV by counting the number of albumin puncta within the vasculature area. Diffusion of fluorescently-labelled mouse IgG in the brain was analyzed from 3

whole OB images acquired on a Zeiss AxioImager microscope. Mean fluorescence intensity was obtained from glomerular and granular regions of the OB sections in both hemispheres and averaged across sections for each animal. Albumin-AlexaFluor594, biocytin-TMR, and AlexaFluor488-IgG fluorescence intensity measures were normalized to vascular density in the same brain regions (images), then to the fluorescence intensity in liver sections to control for the volume of the tracer injected into the blood stream per each mouse. Glomerular and granular FOV were measured and analyzed independently from each other.

ELISA: Total IgG was quantified using the IgG (Total) Mouse Uncoated ELISA Kit (ThermoFisher, 88-50400-22) according to manufacturer's instructions. Primary sera were diluted in PBS with 1% bovine serum albumin (BSA).

Western blotting: Brains were collected from mice after perfusion with PBS. Collected tissue was homogenized in lysis buffer containing protease and phosphatase inhibitors, using a tissue douncer followed by sonication. Specific protein levels were measured by fluorescent Western blotting analysis from 50 μg of brain lysate and quantitation was performed using the LI-COR system (LI-COR, Lincoln, NE) as described (8, 9). The following primary antibodies were used for Western blotting: anti-ZO-1 (1:1000, ThermoFisher Scientific), anti-Occludin (1:250, ThermoFisher), anti-Cadherin-5 (1:500, Abcam), and anti-Caveolin-1 (1:1000, Abcam). Bands for proteins of interest were normalized to β-actin (1:10,000, Novus NB600-501). Primary antibodies were detected with secondary antibodies conjugated to IR-Dye680 and IR-Dye800 (LI-COR 925-32210, 1:20,000). Imaging and quantification were performed using the LI-COR fluorescence Western Blotting instrument and software (8, 9). Measurements of GAS-directed antibody production were performed using an adapted Western blot protocol similar to (6). GAS protein lysates (22 μg per lane) were separated by gel electrophoresis and transferred to a PVDF membrane. Individual lanes were cut and incubated separately with primary sera overnight at 4°C. Sera samples from individual mice were diluted 1:100 after normalization to total IgG level, as determined by ELISA. Antibodies reacting with bacterial proteins on the membrane were detected with IR-Dye800CW (LI-COR 925-32210; 1:20,000). Imaging and quantification were performed using the LI-COR fluorescence Western blotting instrument. Serum antibody bands were normalized to total protein, measured with REVERT reversible total protein stain (LI-COR 926-11011).

Olfactory habituation/dishabituation test: Olfactory function was assessed using a habituation-dishabituation test 6 hours after the fifth (final) GAS infection. Mice were habituated singly to a clean empty cage in the testing room for 30 minutes prior to testing. They were tested in groups of 2-4 mice and filmed for analysis. For testing, mice were allowed to investigate long-handled Q-tips treated with 10 μl of odorant (diluted 1:100) or vehicle (water) for two minutes per trial, with approximately one minute between trials. Each odorant was presented three times in succession, with water presented first. The following odors were used: almond extract, vanilla extract, ethyl butyrate, and 2-phenylethanol. The experimenter was blinded to the genotype of the mouse and treatment during behavioral scoring.

Electrophysiology: Extracellular unit recordings and analyses of odor-evoked spiking activity in the mitral/tufted (M/T) neurons of the OB were performed in awake, head-fixed mice as described in (10, 11). Briefly, after four infections with PBS or live GAS, mice were surgically fitted with a

custom-machined head plate to allow for awake, head-fixed recording from the OB. Mice were inoculated with an equivalent dose of HK-GAS or PBS for the final infection. Recordings were performed in a liquid dilution, ten-channel olfactometer at 48 hours after the final GAS infection. For recordings, mice were anesthetized with 1% isoflurane in O_2 during the craniotomy and durotomy over one of the OBs. A 32-site polytrode acute probe (A1 × 32-Poly3-5mm-25s-177, Neuronexus, Ann Arbor, MI) was lowered into the posterior OB to the ventromedial M/T neuronal layer, typically at a depth of 1.5 - 2.2 mm and 4° angle with respect to vertical within the coronal plane. Signals were collected through an A32-OM32 adaptor (Neuronexus) connected to a Cereplex digital head stage (Blackrock Microsystems, Salt Lake City UT). Unfiltered signals were digitized at 30 kHz in the head stage and recorded by a Cerebus multichannel data acquisition system (BlackRock Microsystems). Experimental events and respiration signals were acquired at 2 kHz by analogue inputs of the Cerebus system. Respiration was monitored with a microbridge mass airflow sensor (Honeywell AWM3300V, Morris Plains, NJ) positioned directly opposite the nose of the mouse. Prior to recording, the back of the probe was painted with a fluorescent dye (DiI, Life Technologies) and probe position was confirmed post hoc in histological sections (Figure S5A, B). Six monomolecular compounds (stimuli) were used: methyl tiglate [Alfa Aesar (Haverhill, MA) A11964], γ-terpinene [Sigma, 223190-5ML], 2-hexanone [Fluka (Mexico), 02473], isoamyl acetate [Tokyo Chemical Industry (Cambridge, MA), A0033], ethyl butyrate [Aldrich E15701], and valeraldehyde [Sigma, 110132]. These compounds were diluted in mineral oil and presented for one second using a custom flow-dilution olfactometer at final concentrations of 0.04%, 0.2% and 1% (vol/vol). Fifteen trials per odor concentration stimulus were presented at approximately 10 second inter-trial intervals. Individual units were automatically identified using Spyking-Circus (https://github.com/spyking-circus). A typical recording yielded 19.8 ± 5.5 units (mean ± SD). Analysis of electrophysiology data was performed blind with respect to the genotype of mice in MATLAB (MathWorks, Natick, Massachusetts, USA).

Statistical analyses: Two-way ANOVA followed by Sidak's correction was performed for multiple comparisons, and unpaired Student's t-tests were performed for binary comparisons. Western blots were compared between two groups using unpaired Student's t-tests. Statistical analyses were performed with GraphPad Prism 6.0 Software. All tests were two-sided using a significance level $\alpha=0.05$. For all statistical models and tests described above, the significance is displayed as follows: non-significant is NS; * is $p<0.05$, ** is $p<0.01$, *** is $p<0.001$.

SUPPLEMENTARY FIGURE LEGENDS

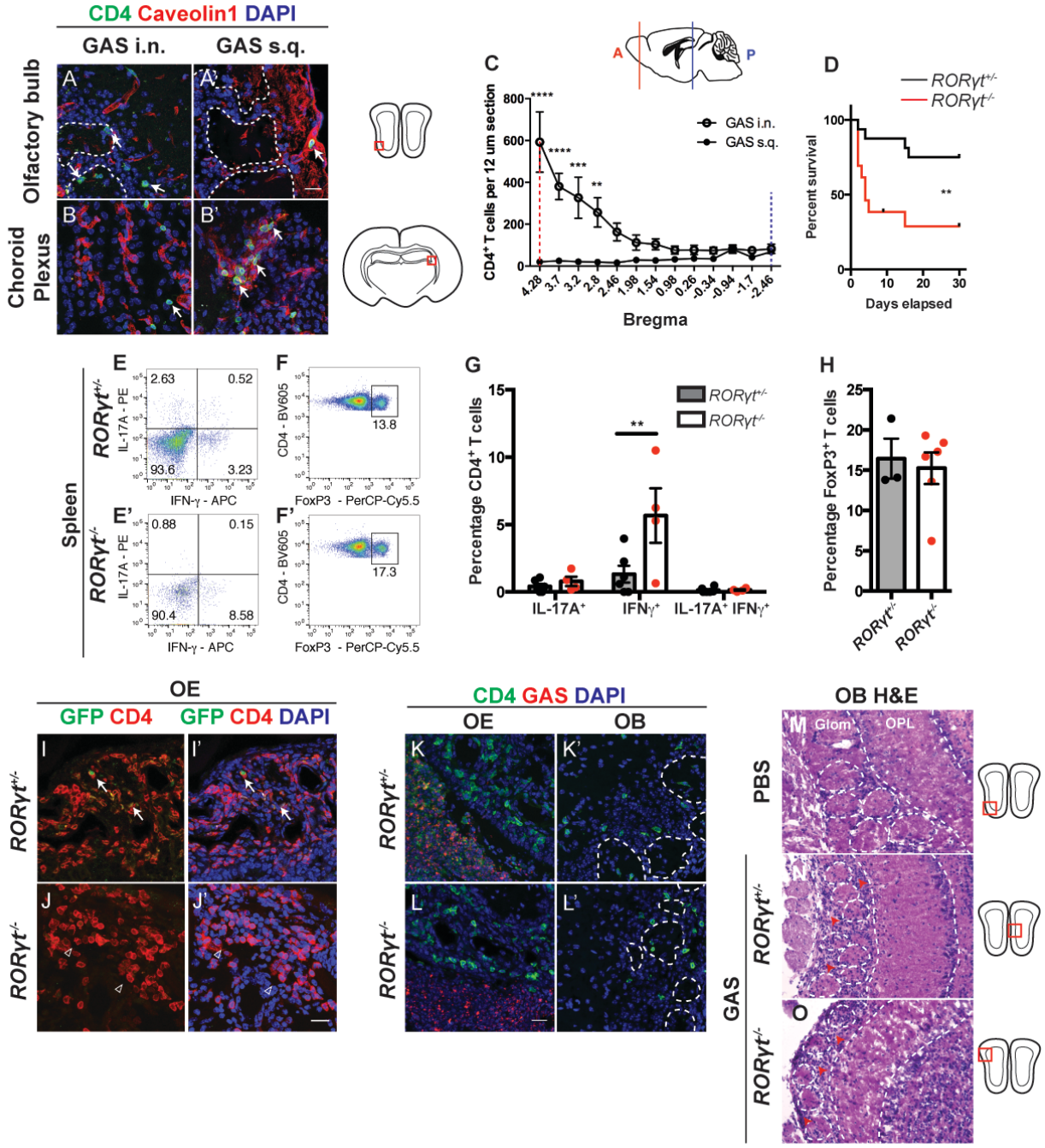

Figure S1. Immunological profiles of CD4$^+$ T cells induced by intranasal GAS infection versus subcutaneous immunization demonstrate that intranasal infections are critical to promote T cell entry into the brain. A-B') Immunofluorescence for CD4 (green, white arrows), Caveolin-1 (red) and DAPI (blue) in the olfactory bulb (OB) and choroid plexus [as denoted by cartoons on the right] of SJL/J mice either infected intranasally (i.n.) with live GAS or immunized subcutaneously (s.c.) with GAS/CFA homogenate. **C)** Quantification of CD4$^+$ T cell distribution along the anteroposterior axis of the brain following i.n. infection (open circles) vs. s.c. immunization (closed circles). X axis represents distance from the bregma and y axis shows CD4$^+$

T cell numbers per 12 μm section. Dashed red and blue vertical lines represent relative positions in the brain cartoon (solid lines). Data were collected from $n = 5$ i.n. and $n = 5$ s.c. mice, represented as mean ± SEM (bregma +4.28, ****P<0.0001; +3.7, ****P<0.0001; +3.2, ***P=0.0002; +2.8, **P=0.010 using ANOVA followed by Bonferroni's *post hoc* correction). $CD4^+$ T cell numbers are elevated in anterior brain regions and choroid plexus after i.n. GAS infections, whereas s.c. immunizations induce recruitment of $CD4^+$ T cells only in the choroid plexus. Thus, multiple i.n. infections with live GAS are critical to induce the entry of $CD4^+$ T cells into the CNS parenchyma. **D)** Kaplan-Meier survival curves for *RORγt*$^{+/-}$ and *RORγt*$^{-/-}$ mice after multiple GAS infections. *RORγt*$^{-/-}$ mice are more vulnerable to death from GAS infection than *RORγ*$^{+/-}$ mice (**p<0.01). **E, E')** Representative FACS plots for cytokine expression in $CD4^+$ lymphocytes from spleens of GAS-infected *RORγt*$^{+/-}$ and *RORγt*$^{-/-}$ mice and **F, F')** $CD4^+$ $FoxP3^+$ regulatory T cells (Treg) splenocytes from GAS-infected *RORγt*$^{+/-}$ and *RORγt*$^{-/-}$ mice. Splenic $CD4^+$ lymphocytes are not activated and there is no significant expansion of the Treg population after multiple GAS infections. **G)** Quantitative cytokine profile analysis of $CD4^+$ splenocytes from GAS-infected *RORγt*$^{+/-}$ and *RORγt*$^{-/-}$ mice. Data are represented as mean ± SEM from n=6 GAS *RORγt*$^{+/-}$ and n=4 GAS *RORγt*$^{-/-}$ mice (IL-$17A^+$, P=0.9797 [non-significant (NS)]; IFN-γ^+, **P=0.0011; IL-$17A^+$ IFN-γ^+, P>0.9999 by two-way ANOVA followed by Sidak's *post hoc* correction). **H)** Quantification of $FoxP3^+$ Treg populations in $CD4^+$ splenocytes from *RORγt*$^{+/-}$ and *RORγt*$^{-/-}$ mice. Data are represented as mean ± SEM from n=3 GAS *RORγt*$^{+/-}$ and n=6 GAS *RORγt*$^{-/-}$ mice, P=0.4772 (NS) by unpaired two-tailed Student's t-test. These data demonstrate that Th17 lymphocytes or INFγ^+ Th17 lymphocytes are absent in spleens of *RORγt*$^{+/-}$ and *RORγt*$^{-/-}$ mice after multiple i.n. GAS infections in contrast to their abundance in the NALTs and brains of *RORγt*$^{+/-}$ mice. **I-J')** Immunofluorescence for GFP (Th17 reporter), CD4 (red) and DAPI (blue) in the olfactory epithelia (OE) from *RORγt*$^{+/-}$ and *RORγt*$^{-/-}$ mice after multiple GAS infections. $CD4^+$ GFP^+ Th17 cells (arrows) are abundant in *RORγt*$^{+/-}$ mice, but no GFP^+ $CD4^+$ cells are seen in *RORγt*$^{-/-}$ OE (open arrowheads). **K, L')** Immunofluorescence for CD4 (green), GAS bacteria (red) and DAPI demonstrates that infection is confined to the OE, with no bacteria present in the OB, for both genotypes. **M-O)** Hematoxylin & eosin staining of OB tissue sections show a large number of cellular infiltrates (red arrows) in the glomerular layer (Glom) of the OB in GAS-infected *RORγt*$^{+/-}$ and *RORγt*$^{-/-}$ mice, but not in PBS controls. The glomerular (Glom) and outer plexiform layers (OPL) of the OB are marked with dashed white lines and the glomeruli are outlined with dashed white ovals. The cartoons on the right show the location where the H&E images were acquired in the OB for each experiment and genotype. Scale bars = 20 μm.

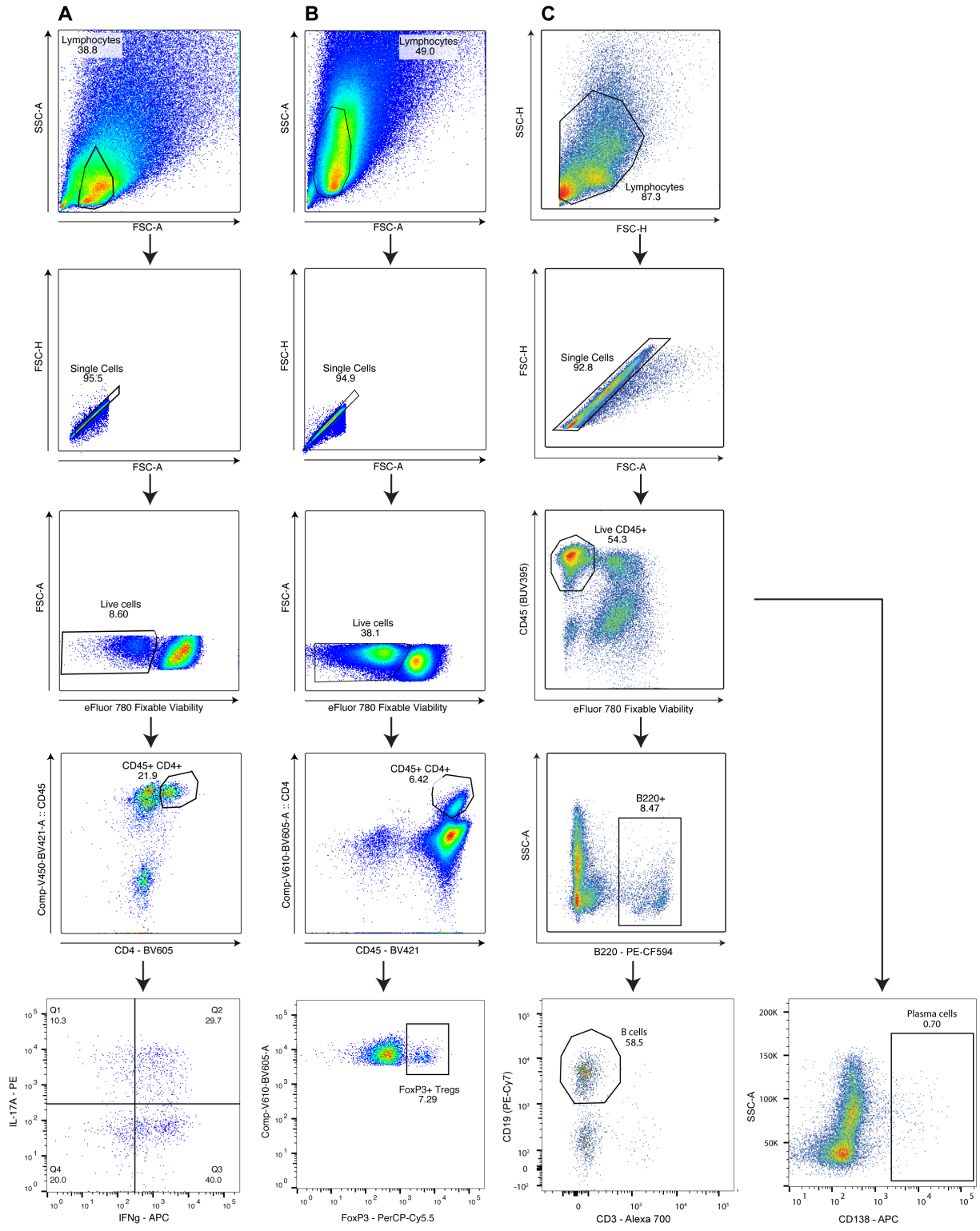

Figure S2. **Gating strategy for FACS sorting of CD4$^+$ Th17, Th1, Treg and B lymphocytes and plasma cells from GAS-infected *RORγt*$^{+/-}$ and *RORγt*$^{-/-}$ mice.** The various lymphocyte populations were distinguished using the following markers: **A**) CD4$^+$ Th17 (IL-17A$^+$), Th1 (IFN-

γ+) and IFN-γ+ Th17 (IL-17A+; IFN-γ+) lymphocytes, **B**) Treg (FoxP3+) lymphocytes, and **C)** B lymphocytes and plasma cells in both GAS-infected *RORγt*$^{+/-}$ and *RORγt*$^{-/-}$ mice.

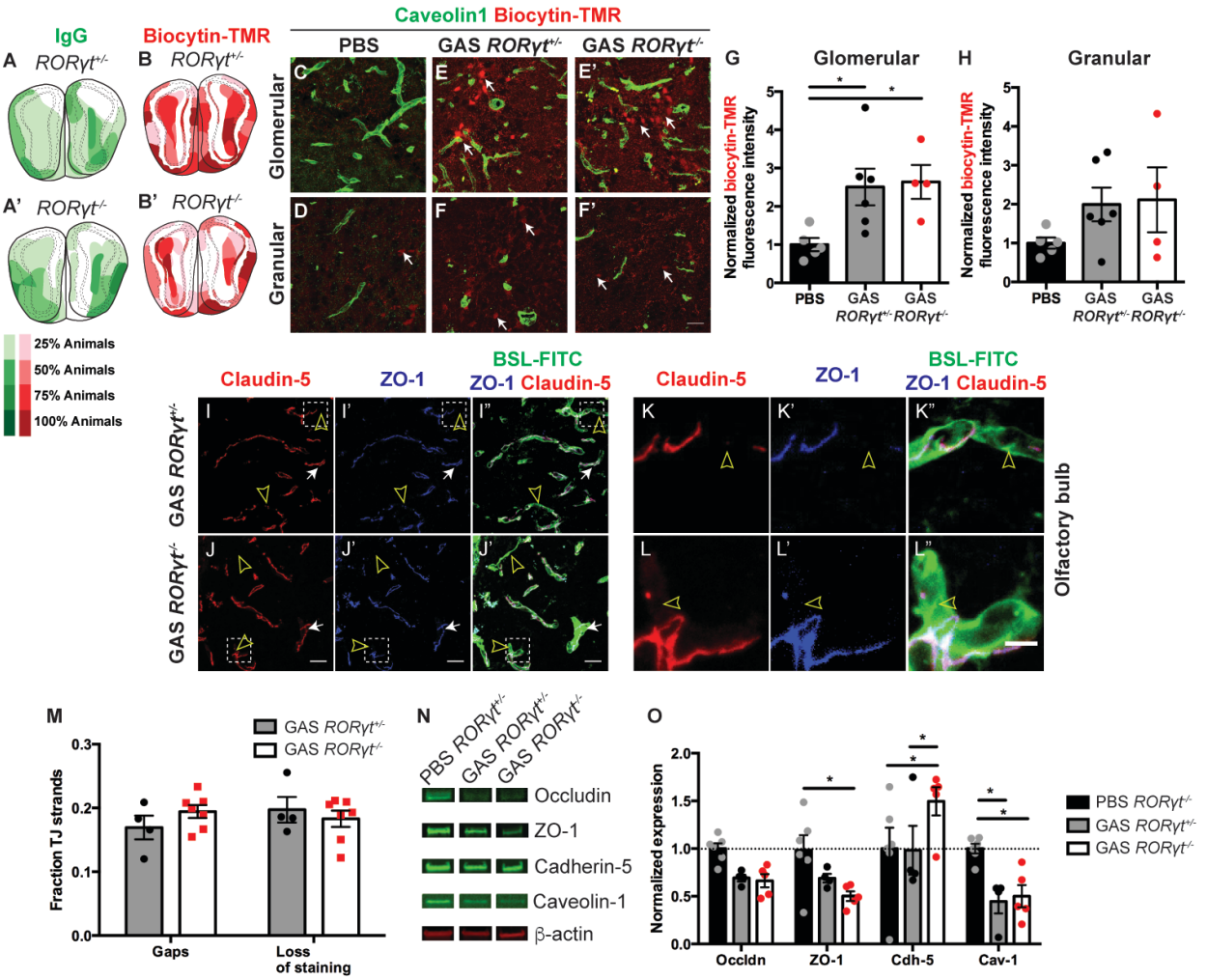

Figure S3. Tight junction protein levels, localization and function are abnormal after multiple GAS infections in both *RORγt*$^{+/-}$ and *RORγt*$^{-/-}$ mice. A, A') Heat maps indicating areas of the olfactory bulb (OB) with serum IgG deposition in GAS-infected *RORγt*$^{+/-}$ or *RORγt*$^{-/-}$ mice. Darker green indicates a higher percentage of mice with serum IgG extravasation in that region. **B, B')** Heat maps indicating areas of the OB with biocytin-TMR tracer deposition in GAS-infected *RORγt*$^{+/-}$ or *RORγt*$^{-/-}$ mice. Darker red indicates a higher percentage of mice with biocytin-TMR extravasation in that region. The areas of serum IgG or biocytin-TMR leakage in the OB are not very different between the two genotypes after multiple i.n. GAS infections. **C-F')** Immunofluorescence for Caveolin-1 (blood vessel marker) and biocytin-TMR in the glomerular or granular OB regions of PBS control mice or GAS-infected *RORγt*$^{+/-}$ or *RORγt*$^{-/-}$ mice. PBS control mice show no tracer deposition in either the **C)** glomerular or **D)** granular layers of the OB. GAS-infected mice show significant biocytin-TMR uptake by neurons (arrows) in both genotypes

in the **E, E')** glomerular and **F, F')** granular OB layers. **G, H**) Quantification of biocytin-TMR staining intensity in the **G)** glomerular and **H)** granular layers of the OB. Data were collected from n=5 PBS, n=6 GAS *RORγt*$^{+/-}$, and n=4 GAS *RORγt*$^{-/-}$ mice, represented as mean ± SEM. **G)** **P*=0.0431, PBS vs. GAS *RORγt*$^{+/-}$; **P*=0.047, PBS vs. GAS *RORγt*$^{-/-}$; *P*=0.97 [non-significant (NS)], GAS *RORγt*$^{+/-}$ vs. *RORγt*$^{-/-}$ by ANOVA followed by Tukey's *post hoc* correction. **H)** No significant differences are found between PBS vs. GAS *RORγt*$^{+/-}$, PBS vs. GAS *RORγt*$^{-/-}$ nor GAS *RORγt*$^{+/-}$ vs. *RORγt*$^{-/-}$ by ANOVA followed by Tukey's *post hoc* correction. **I-L")** Immunofluorescence for tight junction (TJ) proteins Claudin-5 (red), ZO-1 (blue) and blood vessels (BSL-FITC, green) in GAS-infected *RORγt*$^{+/-}$ and *RORγt*$^{-/-}$ OBs. TJ strands show similar structural abnormalities in both GAS-infected *RORγt*$^{+/-}$ and *RORγt*$^{-/-}$ vessels (white arrows indicate gaps in TJ strands, yellow arrowheads indicate extensive loss of TJ strands in blood vessels). **K-L")** Larger magnification images from boxed areas in **I** and **J**. Yellow arrowheads indicate absence of TJ proteins in capillaries. Scale bars = 20 μm in **I-J"**, 5 μm in **K-L". M)** Quantification of the fraction of aberrant TJ strands per field of view in n=4 GAS *RORγt*$^{+/-}$ and n=7 GAS *RORγt*$^{-/-}$ mice, expressed as mean ± SEM. There is no significant difference in the fraction of TJ strands with abnormalities between the two genotypes by two-way ANOVA followed by Sidak's correction for multiple comparisons. **N)** Western blots for selected adherens and tight junction proteins and transcytosis proteins. β-actin is used as a loading control. **O)** Quantification of TJ and caveolar protein levels was done after normalization within β-actin first, followed by comparison to mean PBS levels. Data were collected from n=6 PBS, n=4 GAS *RORγt*$^{+/-}$, and n=5 GAS *RORγt*$^{-/-}$, expressed as mean ± SEM. Occludin: *P*=0.2525 (NS), PBS vs GAS *RORγt*$^{+/-}$; *P*=0.1571 (NS), PBS vs GAS RORγt$^{-/-}$; *P*=0.9883 (NS) GAS *RORγt*$^{+/-}$ vs GAS *RORγt*$^{-/-}$; ZO-1: *P*=0.2841 (NS), PBS vs GAS *RORγt*$^{+/-}$; **P*=0.0266, PBS vs GAS *RORγt*$^{-/-}$; *P*=0.6153 (NS), GAS *RORγt*$^{+/-}$ vs GAS *RORγt*$^{-/-}$; Cadherin-5: *P*=0.9955 (NS), PBS vs GAS *RORγt*$^{+/-}$; **P*=0.0217, PBS vs GAS *RORγt*$^{-/-}$; **P*=0.0341, GAS *RORγt*$^{+/-}$ vs GAS *RORγt*$^{-/-}$; Caveolin-1: **P*=0.0157, PBS vs GAS *RORγt*$^{+/-}$; **P*=0.0209, PBS vs GAS *RORγt*$^{-/-}$; *P*=0.9601 (NS), GAS *RORγt*$^{+/-}$ vs GAS *RORγt*$^{-/-}$ by two-way ANOVA followed by Sidak's correction for multiple comparisons.

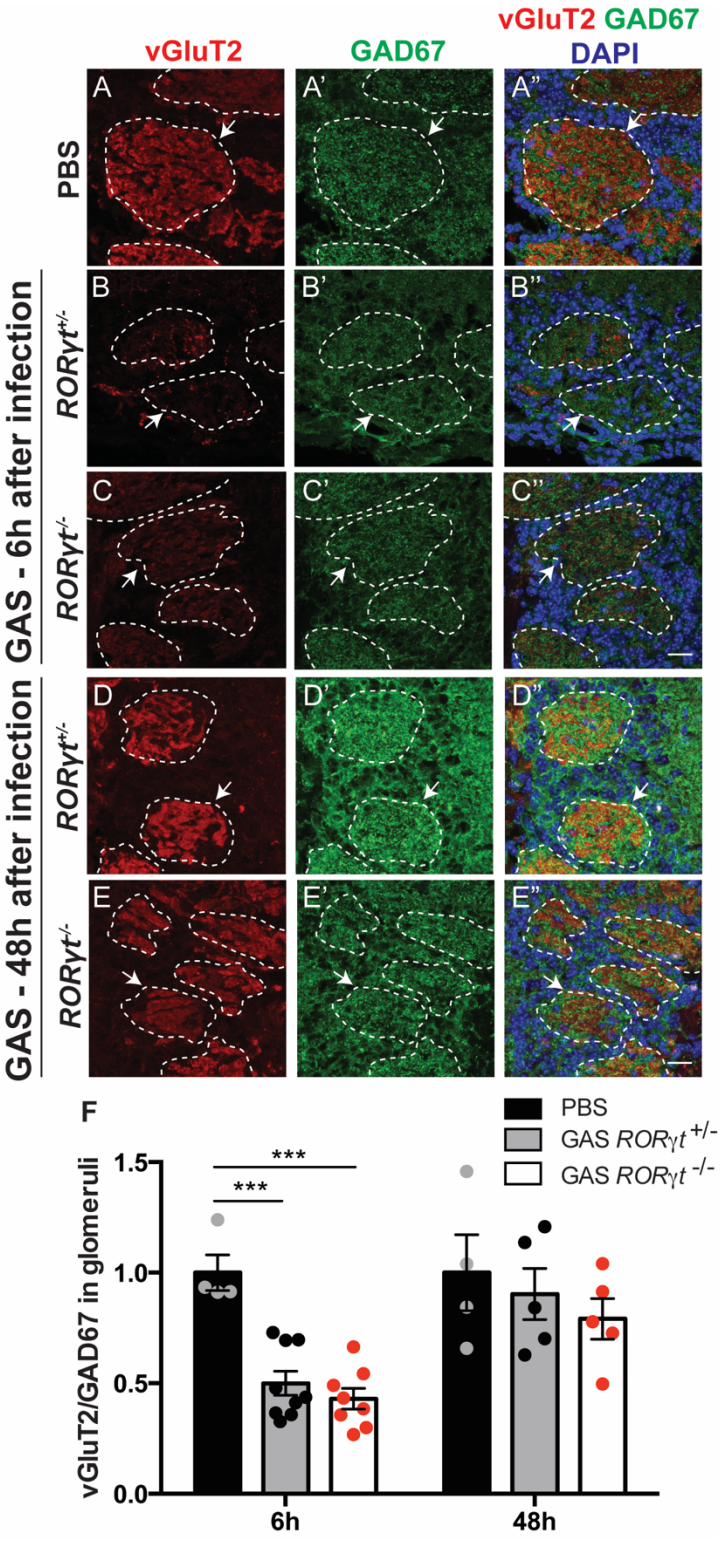

Figure S4. Transient loss of excitatory synaptic proteins in the OB after multiple GAS infections in both *RORγt*$^{+/-}$ and *RORγt*$^{-/-}$ mice. A-A") Glutamatergic (vGluT2^{+}; red) olfactory sensory axon terminals converge and synapse with local interneuron and PG cell dendrites expressing GAD67 (green) in the OB glomeruli [defined by DAPI (blue) and white dashed ovals] in control brains (white arrows). **B-C")** Recurrent GAS infections cause selective loss of vGluT2 staining within glomeruli at 6 hours after the last infection in both *RORγt*$^{+/-}$ and *RORγt*$^{-/-}$ mice, with no change in GAD67. **D-E")** vGluT2 (red) expression is restored within the glomeruli at 48 hours after the last GAS infection in both *RORγt*$^{+/-}$ and *RORγt*$^{-/-}$ mice, with no change in GAD67 (green). **F)** Quantification of vGluT2/GAD67 fluorescence intensity ratios in the glomeruli of PBS or GAS mice in various genotypes at 6 and 48 hours after the last infection. Data were collected from n=4 PBS, n=9 GAS *RORγt*$^{+/-}$ (6h), n=8 *RORγt*$^{-/-}$ mice (6h), n=5 GAS *RORγt*$^{+/-}$ (48h), n=5 *RORγt*$^{-/-}$ mice (48h), represented as mean ± SEM. [**P=0.0059, PBS vs. GAS *RORγt*$^{+/-}$ (6h); *P=0.016 PBS vs. GAS *RORγt*$^{-/-}$ (6h); P=0.8625 [non-significant (NS)] GAS *RORγt*$^{+/-}$ (6h) vs. GAS *RORγt*$^{-/-}$ (6h); P=0.8636 (NS), PBS vs. GAS *RORγt*$^{+/-}$ (48h); P=0.3562 (NS) PBS vs. GAS *RORγt*$^{-/-}$ (48h); P=0.7720 (NS) GAS *RORγt*$^{+/-}$ (48h) vs. GAS *RORγt*$^{-/-}$ (48h); one-way ANOVA followed by Tukey's *post hoc* correction]. Scale bars = 20 µm.

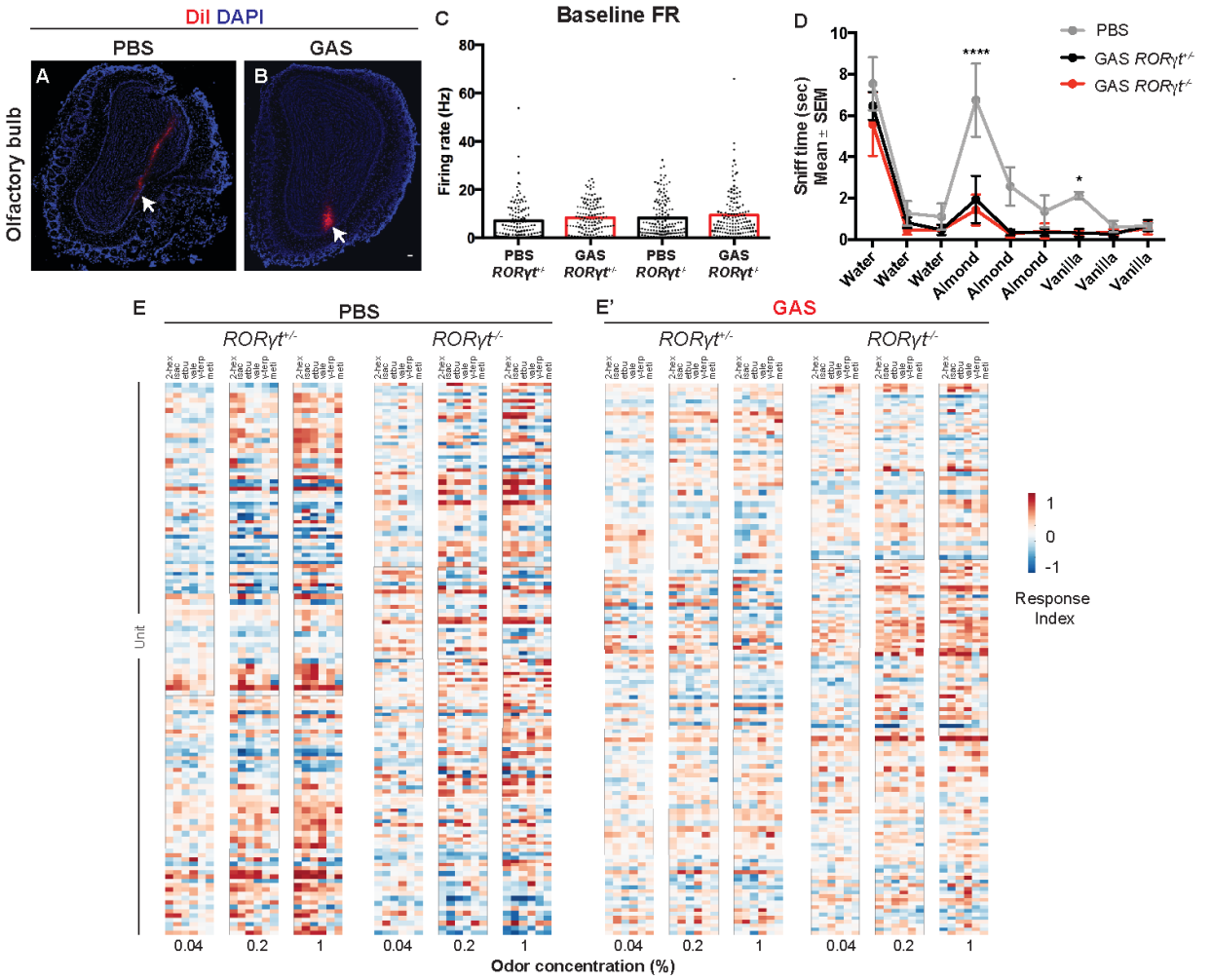

Figure S5. Physiological recording parameters are normal between *RORγt*$^{+/-}$ and *RORγt*$^{-/-}$ mice in either the absence or presence of intranasal GAS infection, despite differences in odor processing. **A, B**) Fluorescence images of olfactory bulbs (OBs) with DiI [$DiIC_{18}(3)$, red, painted on probe face before recording] and DAPI (blue) confirm the placement of the recording probe tip (white arrow) within the mitral/tufted (M/T) neuronal cell layer of the OB in both PBS and GAS-infected mice. **C**) The firing rate during the first inhalation after presentation of mineral oil (control odor) does not differ among groups, indicating that mitral/tufted neurons preserve their baseline function regardless of the genotype (*RORγt*$^{+/-}$, *RORγt*$^{-/-}$) and infection state [PBS (control), GAS(infected)]. Data were collected from n=120 neurons over 6 recordings for 4 PBS *RORγt*$^{+/-}$ mice, n=140 neurons over 7 recordings from 4 PBS *RORγt*$^{-/-}$ mice, n=130 neurons over 7 recordings for 5 GAS *RORγt*$^{+/-}$ mice, and n=144 neurons over 7 recordings for 5 GAS *RORγt*$^{-/-}$ mice, represented as mean ± SEM. There are no significant differences in pairwise comparisons between PBS and GAS *RORγt*$^{+/-}$ or *RORγt*$^{-/-}$ mice, using the Kruskall-Wallis test with Dunn's multiple comparisons test. **D**) A habituation-dishabituation task illustrates the inability of multiple GAS-infected mice to detect changes in odor identity regardless of the genotype at 6 hours after the final GAS infection. Data are mean ± SEM (n=5 PBS, n=6 GAS *RORγt*$^{+/-}$ and n=5 GAS *RORγt*$^{-/-}$ mice). **E, E'**) Heatmaps for relative responses of individual mitral/tufted neurons across three concentrations (0.04%, 0.2% and 1% column blocks) of six monomolecular odors (sub-columns),

with matched cells across a row within genotype. PBS control mice of both genotypes show increased responses (more intense red versus blue) with increasing odor concentration, whereas GAS-infected *RORγt*$^{+/-}$ mitral neurons show no increase in response with higher odor concentrations. GAS-infected *RORγt*$^{-/-}$ neurons show some restoration of concentration-dependent responses to odors.

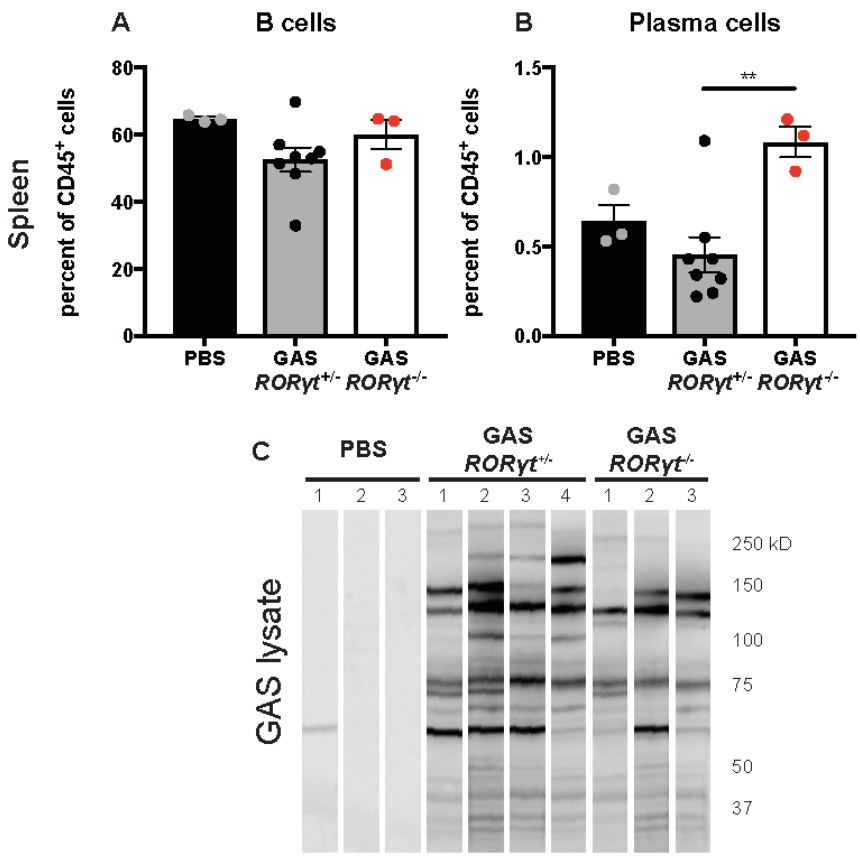

Figure S6. GAS-directed antibody production is normal in *RORγt*$^{-/-}$ mice. A, B) Quantification of the fraction of CD45^{+} B lymphocytes (CD19^{+}) and CD45^{+} plasma cells (CD138^{+}) in spleens of PBS or GAS-infected *RORγt*$^{+/-}$ and *RORγt*$^{-/-}$ mice. B lymphocytes represent a stable population of splenocytes in PBS and GAS-infected *RORγt*$^{+/-}$ and *RORγt*$^{-/-}$ mice. Plasma cells are increased in spleens of GAS-infected *RORγt*$^{-/-}$ compared to either PBS or GAS-infected *RORγt*$^{+/-}$ mice. Data are collected from n=3 PBS, n=8 GAS *RORγt*$^{+/-}$, and n=3 GAS *RORγt*$^{-/-}$ mice and presented as mean ± SEM; **p<0.01. **C)** Western blot analysis of GAS-specific antibodies that are present in GAS-infected mice, regardless of the genotype, but not in PBS controls. Measurements of GAS-directed antibody production was performed using an adapted Western blot protocol. GAS protein lysates (22 µg per lane) were run out in a gel electrophoresis and transferred to a PVDF membrane. Individual lanes were cut apart and incubated separately with primary sera overnight at 4°C. Sera from GAS-infected mice react with GAS proteins immobilized on a PVDF membrane regardless of the genotype (*RORγt*$^{+/-}$ and *RORγt*$^{-/-}$ mice). Each lane represents binding of serum collected from one mouse to the same amount of total GAS protein per lane (22 µg per lane).

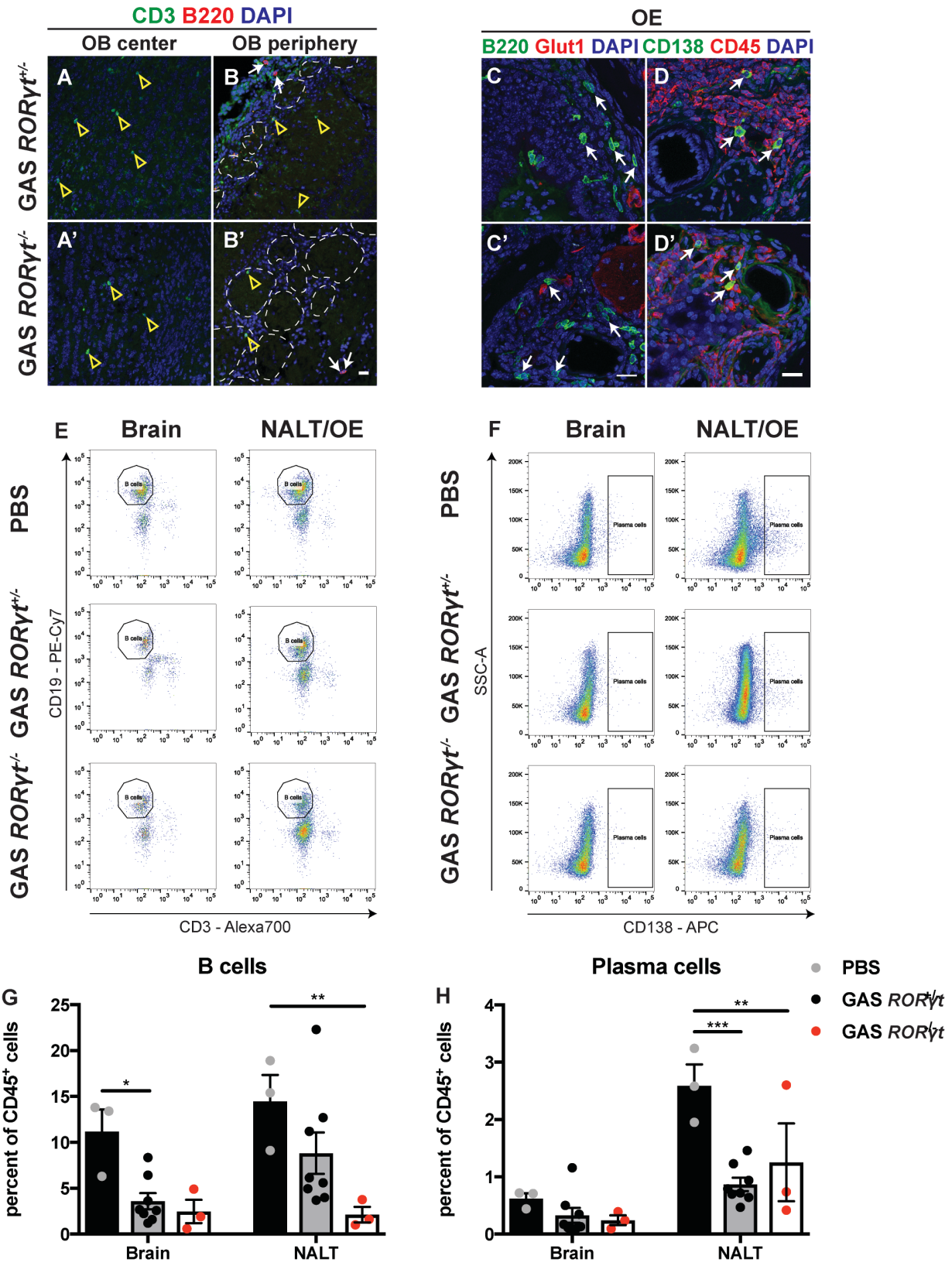
CD3 B220 DAPI
OB center
OB periphery
A
B
A'
B'
GAS RORγt+/-
GAS RORγt-/-
OE
B220 Glut1 DAPI CD138 CD45 DAPI
C
D
C'
D'
E
Brain
NALT/OE
PBS
GAS RORγt+/-
GAS RORγt-/-
CD19 - PE-Cy7
CD3 - Alexa700
B cells
F
Brain
NALT/OE
SSC-A
CD138 - APC
Plasma cells
G
B cells
percent of CD45+ cells
Brain
NALT
H
Plasma cells
PBS
GAS RORγt+/-
GAS RORγt-/-

Figure S7. B cells and plasma cells are absent from the brain parenchyma after multiple i.n. GAS infections. A-B') Immunofluorescence for CD3 (T cells, green), B220 (CD45R, B cells, red) and DAPI (blue, nuclei) in the olfactory bulb (OB) from GAS-infected *RORγt*$^{+/-}$ and *RORγt*$^{-/-}$ mice. B cells are present only in brain meninges, while T cells infiltrate throughout the OB in the glomerular layer (white oval circles). **C-C')** Immunofluorescence for B220 (green) and Glut1 (red) shows B cell populations present throughout the olfactory epithelium (OE) in both genotypes after GAS infections. **D-D')** Immunofluorescence of OE for CD138 (plasma cells, green) and CD45 (activated lymphocytes, red) shows presence of some plasma cells and many lymphocytes in OE in GAS-infected *RORγt*$^{+/-}$ and *RORγt*$^{-/-}$ mice. **E, F)** Representative FACS plots of B220^{+} CD19^{+} B lymphocytes and CD138^{+} plasma cells purified from brain (left) and NALT/OE (right) from PBS control, GAS-infected *RORγt*$^{+/-}$ and *RORγt*$^{-/-}$ mice. **G, H)** Quantification of the fraction of CD19^{+} B220^{+} B cell populations in the OB and NALT and CD138^{+} plasma cell populations in brain and NALT shows that these cell types are unchanged between GAS-infected *RORγt*$^{+/-}$ and *RORγt*$^{-/-}$ mice. Data were collected from n=3 PBS, n=8 GAS *RORγt*$^{+/-}$ and n=3 *RORγt*$^{-/-}$ mice represented as mean ± SEM. (**G**) **P*=0.0471, PBS vs. GAS *RORγt*$^{+/-}$; ***P*=0.065 PBS vs. GAS *RORγt*$^{-/-}$; **H**) ****P*=0.0001 PBS vs. GAS *RORγt*$^{+/-}$; ***P*=0.0086 PBS vs. GAS *RORγt*$^{-/-}$; one-way ANOVA followed by Tukey's *post hoc* correction). Scale bars = 20 μm.

SUPPLEMENTARY REFERENCES

1. M. Ciofani *et al.*, A validated regulatory network for Th17 cell specification. *Cell* **151**, 289-303 (2012).
2. Ivanov, II *et al.*, The orphan nuclear receptor RORgammat directs the differentiation program of proinflammatory IL-17+ T helper cells. *Cell* **126**, 1121-1133 (2006).
3. T. Dileepan *et al.*, Group A Streptococcus intranasal infection promotes CNS infiltration by streptococcal-specific T cells. *J Clin Invest* **126**, 303-317 (2016).
4. L. Brimberg *et al.*, Behavioral, pharmacological, and immunological abnormalities after streptococcal exposure: a novel rat model of Sydenham chorea and related neuropsychiatric disorders. *Neuropsychopharmacology* **37**, 2076-2087 (2012).
5. K. Yaddanapudi *et al.*, Passive transfer of streptococcus-induced antibodies reproduces behavioral disturbances in a mouse model of pediatric autoimmune neuropsychiatric disorders associated with streptococcal infection. *Mol Psychiatry* **15**, 712-726 (2010).
6. K. L. Hoffman, M. Hornig, K. Yaddanapudi, O. Jabado, W. I. Lipkin, A murine model for neuropsychiatric disorders associated with group A beta-hemolytic streptococcal infection. *J Neurosci* **24**, 1780-1791 (2004).
7. S. E. Lutz *et al.*, Caveolin1 Is Required for Th1 Cell Infiltration, but Not Tight Junction Remodeling, at the Blood-Brain Barrier in Autoimmune Neuroinflammation. *Cell Rep* **21**, 2104-2117 (2017).
8. D. Knowland *et al.*, Stepwise recruitment of transcellular and paracellular pathways underlies blood-brain barrier breakdown in stroke. *Neuron* **82**, 603-617 (2014).
9. J. E. Lengfeld *et al.*, Endothelial Wnt/beta-catenin signaling reduces immune cell infiltration in multiple sclerosis. *Proc Natl Acad Sci U S A* **114**, E1168-E1177 (2017).
10. K. A. Bolding, K. M. Franks, Complementary codes for odor identity and intensity in olfactory cortex. *Elife* **6** (2017).
11. K. A. Bolding, K. M. Franks, Recurrent cortical circuits implement concentration-invariant odor coding. *Science* **361** (2018).